Soft-Chemical Synthetic Route to Superparamagnetic FeAs@C Core–Shell Nanoparticles Exhibiting High Blocking Temperature

ARTICLE *in* CHEMISTRY OF MATERIALS · MARCH 2013

Impact Factor: 8.35 · DOI: 10.1021/cm303632c

5 AUTHORS, INCLUDING:

Prachi Desai
Missouri University of Science and Technology
5 PUBLICATIONS **7** CITATIONS
SEE PROFILE

Jakub Adam Koza
Missouri University of Science and Technology
41 PUBLICATIONS **510** CITATIONS
SEE PROFILE

Akshay Pariti
Missouri University of Science and Technology
3 PUBLICATIONS **7** CITATIONS
SEE PROFILE

Manashi Nath
Missouri University of Science and Technology
45 PUBLICATIONS **2,194** CITATIONS
SEE PROFILE

CHEMISTRY OF MATERIALS

Article

pubs.acs.org/cm

Soft-Chemical Synthetic Route to Superparamagnetic FeAs@C Core–Shell Nanoparticles Exhibiting High Blocking Temperature

Prachi Desai,[†,‡] Kai Song,[§,∥] Jakub Koza,[†] Akshay Pariti,[⊥] and Manashi Nath*[,†,‡]

[†]Department of Chemistry, [§]Materials Research Centre, and [⊥]Department of Chemical Engineering, Missouri University of Science and Technology, Rolla, Missouri 65409, United States

Supporting Information

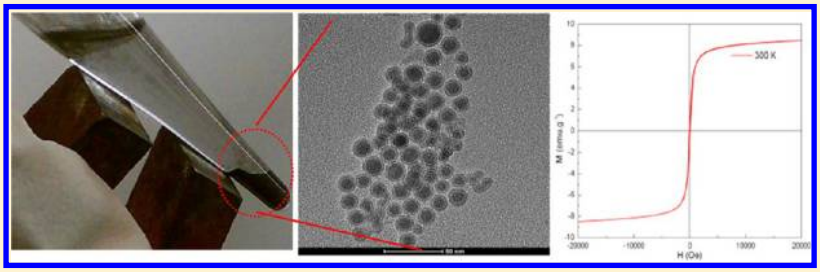

ABSTRACT: Superparamagnetic FeAs nanoparticles with a fairly high blocking temperature (T_B) have been synthesized through a hot injection precipitation technique. The synthesis involved usage of triphenylarsine (TPA) as the As precursor, which reacts with $Fe(CO)_5$ by ligand displacement at moderate temperatures (300 °C). Addition of a surfactant, hexadecylamine (HDA), assists in the formation of the nanoparticles, due to its coordinating ability and low melting point which provides a molten flux like condition making this synthesis a solventless method. Decomposition of the carbonaceous precursors, HDA, TPA and $Fe(CO)_5$, also produces the carbonaceous shell coating the FeAs nanoparticles. Magnetic characterization of these nanoparticles revealed the superparamagnetic nature of these nanoparticles with a perfect anhysteretic nature of the isothermal magnetization above T_B. The T_B observed in this system was indeed high (240 K) when compared with other superparamagnetic systems conventionally utilized for magnetic storage devices. It could be further increased by decreasing the strength of the applied magnetic field. The narrow hysteresis with low magnitude of coercivity at 5 K suggested soft ferromagnetic ordering in these nanoparticle ensembles. Mössbauer and XPS studies indicated that the Fe was present in +3 oxidation state and there was no signature of Fe(0) that could have been responsible for the increased magnetic moment and superparamagnetism. Typically for superparamagnetic nanoparticle ensemble, the need for isolation of the superparamagnetic domains (thereby inhibiting particle aggregation and enhancing the T_B) has been in constant limelight. Carbonaceous coating on these as-synthesized nanoparticles formed *in situ* provided the physical nonmagnetic barrier needed for such isolation. The high T_B and room temperature magnetic moment of these FeAs@C nanoparticles also make them potentially useful for applications in ferrofluids and magnetic refrigeration. In principle this method can be used as a general route toward synthesis of other arsenide nanostructures including the transition metal arsenide which show interesting magnetic and electronic properties (e.g., CoAs, MnAs) with finer control over morphology, composition and structure.

KEYWORDS: *FeAs nanoparticles, superparamagnetic nanoparticles, pnictide superconductors, LiFeAs, triphenylarsine*

The unexpected discovery of superconductivity in LaFePO by Hosono et al. in 2006[1] that led to identification of a new series of iron oxypnictide based superconductors, *Ln*Fe*Pn*O [*Ln* = La, Ce, Sm, Gd, Nd, Pr; *Pn* = P, As],[2−5] has made the iron pnictides a center of attraction to materials scientists. The iron pnictide based superconducting family was further enriched over the last couple of years with the discovery of new compositions, specifically the AFe_2As_2 (*A* = Ba, Sr etc.)[6] and the *A*FeAs (*A* = Li, Na),[7,8] which are generically referred to as [122] and the [111] series respectively, and the parent oxypnictide, *Ln*Fe*Pn*O, is referred to as the [1111] series. The common structural motif in these layered superconductors is the anionic FeAs layer containing the edge shared $FeAs_4$ tetrahedron, which is believed to be responsible for superconductivity.[9,10] The electronic and magnetic properties of these superconductors show a dependence on the geometry of the $FeAs_4$ tetrahedron.[11] While the [1111] series is built up by the alternate stacking of the anionic pnictide layer with the cationic Ln_2O_3 layer, the simpler ternary compositions ([111] and [122] series) contain the alkali or the alkaline earth cations placed between the FeAs layers. In these pnictide superconductors, the magnetic exchange interactions between the Fe atoms within the pnictide layer play a determining factor in defining the superconducting and electronic properties of these superconductors and the binary pnictides might serve as a proxy system to study these exchange interactions. More

Received: November 9, 2012
Revised: March 8, 2013
Published: March 15, 2013

importantly, FeAs nanostructures will be an ideal starting point for the synthesis of nanostructures of these pnictide superconductors through a simple sacrificial template approach.

Bulk FeAs is an interesting antiferromagnetic (T_N = 70 K) semiconductor material.[12] It crystallizes in the orthorhombic MnP structure type[13] and exhibits helimagnetism owing to the characteristic arrangement of the Fe^{3+} spins along the *c*-axis.[14] Recent work on FeAs using neutron diffraction studies insinuates the role of spin-density wave (SDW) filling the gaps in Fermi surface, as a possible explanation for the magnetic ordering below the T_N in this system.[15] Apart from being the backbone of the pnictide superconductors, these attributes also make FeAs very useful in spintronic applications and magnetic storage devices. However, it may be noted that even though several transition metal pnictide, *TmPn* (*Tm* = Fe, Co, Ni, Mn; *Pn* = P, As), nanostructures are known in abundance,[16−22] reports of FeAs nanostructures are very limited to date. Lu et al. have made FeAs nanoparticles sonochemically from transition metal chlorides and arsenic,[23] while Zhang and co-workers made FeAs nanocrystals from reductive recombination of $FeCl_3$ and $AsCl_3$ at 150−180 °C.[24] However, these reports did not provide any details about the magnetic nature of the FeAs nanoparticles, and also the morphology was very ill-defined.

While the high temperature solid state reactions form the most thermodynamically stable form of these pnictides, soft chemical synthesis routes and so-called *chimie douce* methods relying on association at the molecular level might offer the much needed alternative to form the metastable nanostructured phases. Numerous phosphide and chalcogenide nanostructures have been made by the solution based hot-injection method where the precursors are injected into a refluxing solution and the thermal gradient leads to spontaneous nucleation and nanostructure growth.[25] Liquid phase reactions are especially lucrative since they offer a better handle at morphology control and chemical composition of the resulting nanostructures. However, the suitable choice of the reactants and their relative reactivities in the medium play a very definitive role toward the progress of the reaction. The dearth of synthetic strategies toward formation of arsenide nanostructures through solution chemistry is mainly due to the toxicity of many of the volatile As-precursors like $AsCl_3$, AsH_3 and even metallic As, which may be acting as an obstacle. However, recently triphenylarsine (TPA) has been used as As precursor for the growth of InAs and GaAs under solid-state conditions and refluxing in benzene, respectively.[26,27] TPA as a precursor addresses the toxicity related issues and is a much more lucrative As precursor in lieu of its ease of handling, moderate reactivity and less toxicity.

In this paper we discuss a facile one step low-temperature method to synthesize FeAs nanoparticles in high yield by a simple surfactant-assisted arrested precipitation reaction between $Fe(CO)_5$ and triphenylarsine ($(C_6H_5)_3As$, TPA) and reveal the unprecedented superparamagnetic behavior of these nanoparticles with a high blocking temperature (240 K). At the initiation of the reaction, TPA attaches to the Fe center through simple ligand exchange chemistry to form a probable intermediate which might act as the single source precursor, thereby facilitating the low-temperature reaction in the absence of any catalyst. The method reported here does not require additional solvent medium thereby reducing byproducts and simplifying the product purification steps.

EXPERIMENTAL METHODS

Synthesis. The synthesis of FeAs nanoparticles was carried out in a N_2 filled glovebox containing less than 1 ppm of O_2. 1 mM triphenylarsine and 5 mM HDA was weighed and added to a three-neck round-bottom flask equipped with a magnetic stir bar and air condenser. The mixture was slowly heated to 325 °C, during which the reactants slowly melted and the colorless mixture refluxed in its own vapors. 1 mM $Fe(CO)_5$ maintained at room temperature was then injected using a syringe pump into the hot HDA + TPA mixture. Upon addition of $Fe(CO)_5$ the solution immediately turned black with rapid evolution of gases. After 5 min the gases subsided and the black solution was left to reflux for 3 h. After 3 h the heating was stopped and the reaction mixture was cooled down to room temperature.

It should be noted here that the molar ratio for obtaining pure phase FeAs was 1:1:5 for $Fe(CO)_5$:TPA:HDA. If the As is taken in excess of 1:1 with respect to Fe, the nanoparticle shows As-rich composition and the product contains a mixture of iron arsenide phases (e.g., $FeAs_2$ along with FeAs). The effect of varying the surfactant relative ratios has been discussed below (*vide infra*).

The arsenic precursor, TPA, is very favorable in the sense that it is less volatile, melts easily, decomposes at higher temperatures and is, therefore, less hazardous. Moreover, the handling of solid TPA does not require any complicated protocol. However, to reduce the exposure toward As precursors, the entire reaction was performed in a N_2 filled drybox.

Purification. The as-synthesized product, by virtue of its attraction to a magnet, was purified through simple magnetic filtration. The isolated product was washed at least 3−4 times with ethanol and hexane using ultrasonication to remove excess HDA and any unreacted precursors. After centrifugation the powder collected from the bottom of the tube was dried in air. The yield of the product was in excess of 90% with respect to the amount of $Fe(CO)_5$ taken as the precursor. The product was characterized further through powder X-ray diffraction (pxrd), scanning and transmission electron microscopy (SEM and TEM respectively), energy dispersive spectroscopy (EDS), X-ray photoelectron spectroscopy (XPS), atomic absorption spectroscopy (AAS), Raman analysis, Mössbauer and magnetic studies.

Characterization. *PXRD.* The as-synthesized powder was ground and used for PXRD, which was carried out on a Philips Xpert diffractometer scanning from 2θ range 5 to 90°.

SEM, TEM and STEM. A Technai F20 microscope operating at 200 kV was used for TEM while a dual beam Helios FIB microscope was used for SEM and STEM studies. Samples for TEM and STEM were made by dispersing as- synthesized FeAs nanoparticles in ethanol by ultrasonication for 30 min and adding drops from the diluted dispersion on a carbon coated 300 mesh Cu grid followed by drying in air.

XPS. XPS analysis was performed with Kratos Axis 165, with a hemispherical 8 channel analyzer. Photoemission was stimulated with a monochromatic Al source for FeAs@C nanoparticles. The XPS spectra of Fe2p and As3d were collected at pass energy of 80 peV. Sputtering was performed for 5 min using argon gas.

Magnetic Measurements. Magnetic moment and isothermal magnetization was collected from a SQUID magnetometer and the vibrating sample magnetization (VSM) option of physical property measurement system (PPMS) respectively. The powdered sample of known mass (13.1 mg) was loaded in a gel cap, which was inserted into the magnetometer with the help of standard sample loader. The diamagnetic signal from the gel cap was collected separately and subtracted as a background from the signal obtained from the sample. The ZFC data was obtained after cooling the sample down under zero magnetic field and then measuring the magnetic susceptibility warming up data by applying a magnetic field in the range of 100−1000 Oe. The FC data was collected as the sample was cooled down under the same applied magnetic field. The isothermal magnetization against applied field was collected at different temperatures ranging from 5 to 350 K by applying magnetic fields from −20000 to 20000 Oe.

Mossbauer. ^{57}Fe Mössbauer experiments were performed in transmission geometry at room temperature using a conventional

dx.doi.org/10.1021/cm303632c | *Chem. Mater.* 2013, 25, 1510−1518

constant acceleration spectrometer and a gamma-ray source of ^{57}Co in a Rh matrix. Velocity calibration and isomer shifts are given with respect to alpha-Fe foil at room temperature. The Mössbauer data was analyzed by Lorentzian line fitting using RECOIL software.[28]

Raman. Raman spectroscopy was performed using the Horiba Jobin Yvon Lab Raman ARAMIS model. The laser used was He−Ne with a power of 17/4. An average of 10 scans was collected.

AA Spectroscopy. AAS was carried out on a Perkin-Elmer spectrometer (2800 model). The sample preparation involved digesting a known quantity of the sample (16.1 mg) in a measured volume of concentrated HNO_3 and filtering to remove any undissolved residue. The standard solutions were made in a similar way by dissolving Fe wire in concentrated HNO_3. The Fe content in the sample was estimated by comparing with the standard.

RESULTS AND DISCUSSION

The formation of the highly crystalline FeAs phase was confirmed by pxrd as shown in Figure 1, which revealed that

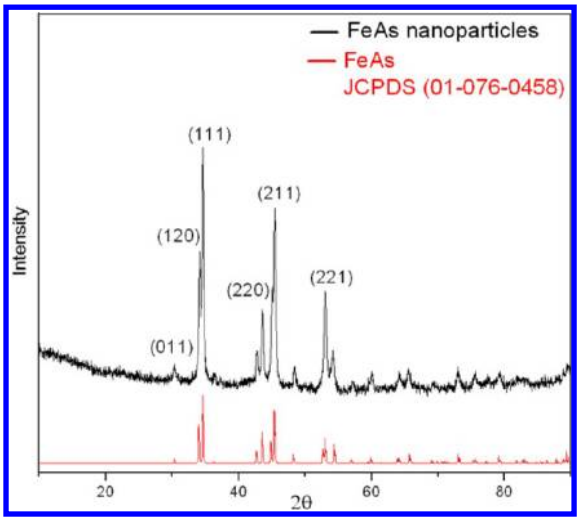

Figure 1. PXRD pattern of the FeAs nanoparticles synthesized at 300 °C.

the as-synthesized nanoparticles crystallized in the MnP structure type (JCPDS file, card number (01-076-0458).[14] The diameter of the nanoparticles as calculated from Scherer equation was 13 nm.[29] No other phase of FeAs or any other impurity was detected. The size of the nanoparticles was dependent on the refluxing time. When the temperature of $Fe(CO)_5$ addition was reduced to 250 °C, a mixture of $FeAs_2$ and FeAs was obtained as seen from the pxrd pattern shown in Supporting Information Figure S1.

Detailed investigations from the STEM and TEM images showed high yield of the nanoparticles in the product and also revealed high degree of monodispersity in the nanoparticle ensemble. Furthermore, microscopic imaging revealed that FeAs nanoparticles were core−shell type as seen in the low magnification STEM image shown in Figures 2A and 2B. The average particle diameter was 10−15 nm, with core sizes being 8−10 nm. The lighter contrast shell is approximately 2−4 nm in thickness. Several wide area SEM images were analyzed to obtain a statistical histogram for the particle size distribution. The histogram showed that the mean size of the core falls well in the range of 8−10 nm as shown in Figure 2C while the particle size distribution was in the range of 10−15 nm (Figure S2 in the Supporting Information). The nanoparticles

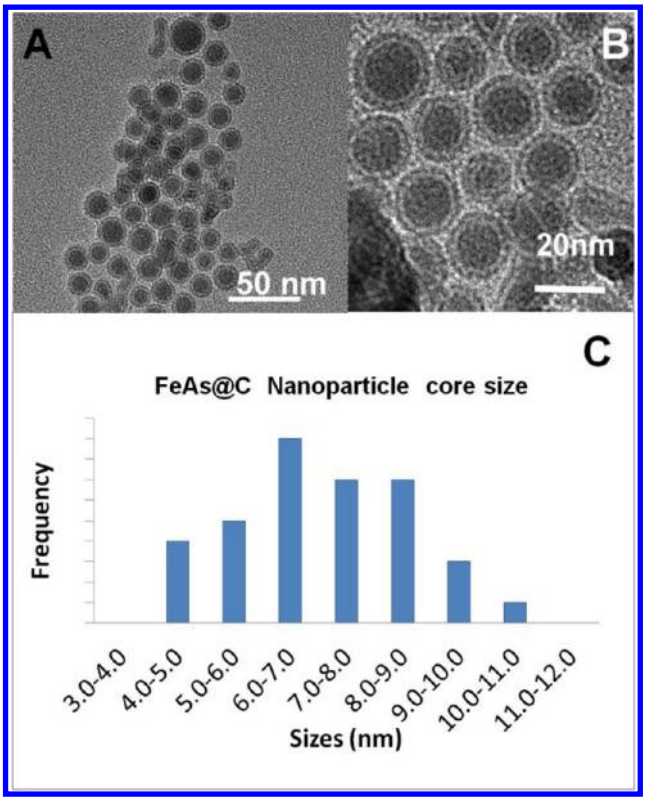

Figure 2. (A, B) STEM images of the nanoparticles showing core−shell nature and ordered arrangement. (C) Histogram analysis for the size distribution of the core in these nanoparticles.

frequently exhibited a hexagonal arrangement on the TEM grids as shown in Figure 2B.

The presence of the surfactant was essential for formation of the nanoparticles. HDA served both as a solvent and as a capping agent. Nitrogen containing coordinating polymers like copoly(styrene-4-vinylpyridine) and copoly(styrene-*N*-vinylpyrrolidone) have long been known to act as nucleophiles and brilliant capping agents.[30] In our opinion HDA also acts similarly to these solvents. Other experiments that involved changing the concentration of HDA indicated that concentration of HDA alters the nanoparticle morphology. When the concentration of HDA was reduced [1:1 for HDA:$Fe(CO)_5$], nanoparticles did not form. An increase in HDA concentration to [10:1 for HDA:$Fe(CO)_5$] gave square shaped nanoparticles. Thus, the role and optimal concentration of HDA were determined as an effective capping agent at 5 mM relative concentration.

The core in these nanoparticles was single crystalline as exhibited by the lattice fringes corresponding to (110) spacing of FeAs as shown in the HRTEM (Figure 3).The selected area electron diffraction (SAED) pattern was also collected over an ensemble of nanoparticles, which, as expected, exhibited a spotty ring pattern typical for a random distribution of small crystallites. SAED could not be performed on individual nanoparticles owing to the particle sizes being very small as compared to the SAED aperture. The shell, on the other hand, did not reveal any crystalline ordering and was mostly amorphous. Compositional analysis of the core and the shell was done through EDS line scan analysis and XPS. The EDS spectrum as shown in Figure 4A verified the presence of Fe and As in the nanoparticles with an approximate ratio of 1:1.3. The XPS analysis (Figure 4B) also confirms the presence of strong

dx.doi.org/10.1021/cm303632c | *Chem. Mater.* 2013, 25, 1510−1518

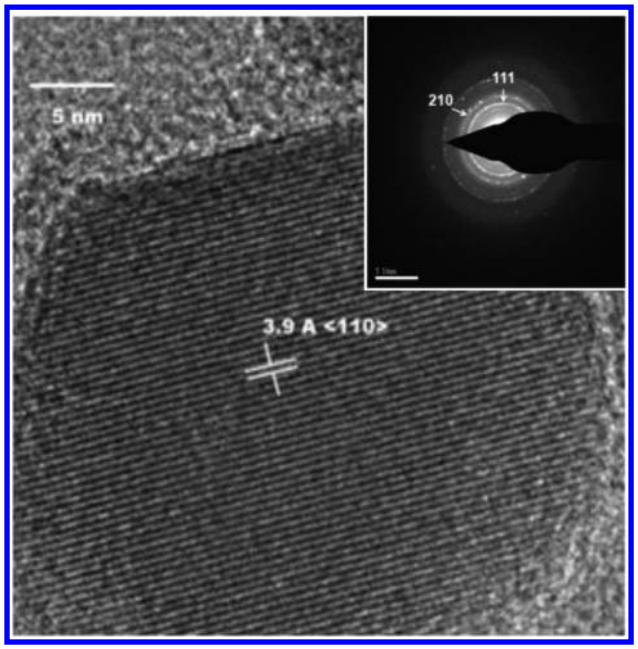

Figure 3. HRTEM image of a nanoparticle showing the crystalline nature of the core and lattice fringes corresponding to FeAs. Inset shows the SAED pattern collected from an ensemble of such nanoparticles.

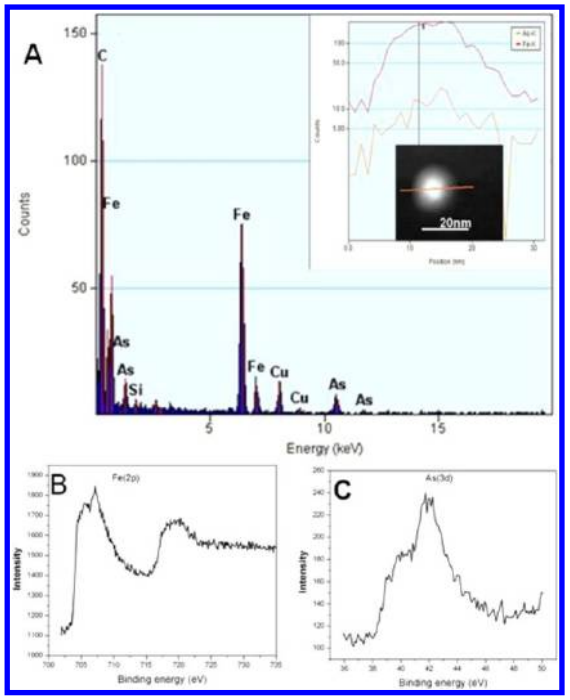

Figure 4. (A) EDS spectrum from the nanoparticles. The inset shows EDS line scan across a single nanoparticle showing both Fe and As in the core. (B, C) XPS analysis of these nanoparticles showing the peaks corresponding to Fe(2p) at 767 eV and As(3d) at 42 eV.

peaks at 767 eV for Fe (2p) and 42 eV for As (3d) respectively. The XPS and EDS spectra collected from individual nanoparticles also picked up significant amounts of C.

To get a better insight into the compositional analysis of the core and the shell of these nanoparticles, detailed elemental mapping was carried out over a single nanoparticle. A line scan performed on a single nanoparticle as shown in the inset of Figure 4A showed that Fe and As peak intensities intensified at the same time in the nanoparticle core and diminished abruptly near the shell with the concentration of both Fe and As being maximum at the center. The carbon signal on the other hand is more concentrated near the shell and is minimal in the core of the nanoparticle (See Figure S3 in the Supporting Information). These corroborated the fact that the FeAs nanoparticles were indeed covered with a carbonaceous shell resulting in the core–shell morphology. Detailed XPS analysis also provided support of this proposed core–shell compositional variance, wherein the Fe (2p) and As (3d) signal increased considerably after sputtering for about 5 min, which removed approximately 2–3 nm from the surface of the nanoparticles, thereby revealing more of the core.

The core and shell composition of these nanoparticles were further studied through Raman spectroscopy. Raman spectra of the FeAs@C nanoparticles showed peaks at 223 cm^{-1}, 288 cm^{-1}, 406 cm^{-1} and 605 cm^{-1} as seen in Figure 5. These bands

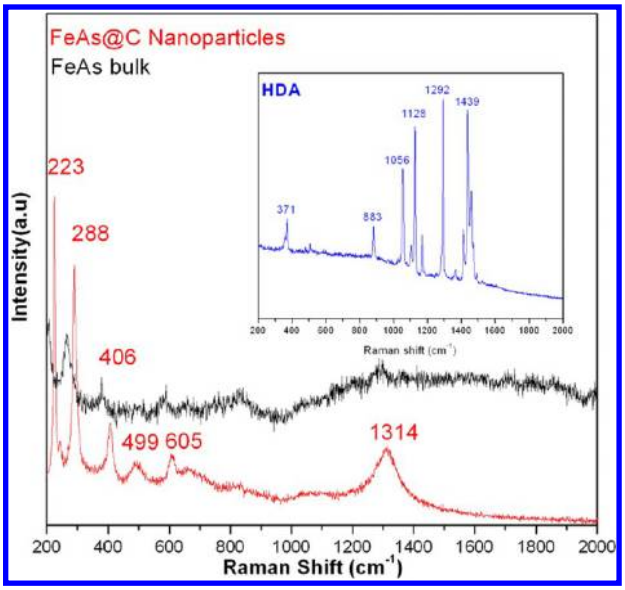

Figure 5. Raman spectrum of FeAs@C nanoparticles compared with that of FeAs bulk. Inset shows the Raman spectrum for HDA.

correspond well with the Raman spectra obtained from bulk FeAs (shown in Figure 5) with a slight shift toward higher wavenumbers as expected for nanostructured morphology.[31] The band observed at 1314 cm^{-1} for the nanoparticle sample, however, was not prominent in bulk FeAs, but is rather a characteristic signature of the D-band of amorphous carbon.[32] It should be noted that the Raman spectrum of the nanoparticles was distinctly different from the spectrum obtained from pure HDA as shown in the inset of Figure 5. Hence the presence of HDA on the shell of these nanoparticles was ruled out and the shell was confirmed to be formed of amorphous carbon.

Magnetic Properties. FeAs has interesting magnetic properties in lieu of the characteristic arrangements of Fe atoms along the *c*-axis leading to helimagnetism.[14] Bulk FeAs is a double helical magnet below T_N = 70 K (T_N is the Neel temperature), where the magnetic moments are at right angles to the spiral axis (common *c*-axis) in the absence of a magnetic field.[14] However, unlike the other pnictides of similar structure type, FeAs exhibits a complex magnetic behavior in its bulk state. The magnetic susceptibility follows the Curie–Weiss law

dx.doi.org/10.1021/cm303632c | *Chem. Mater.* 2013, 25, 1510–1518

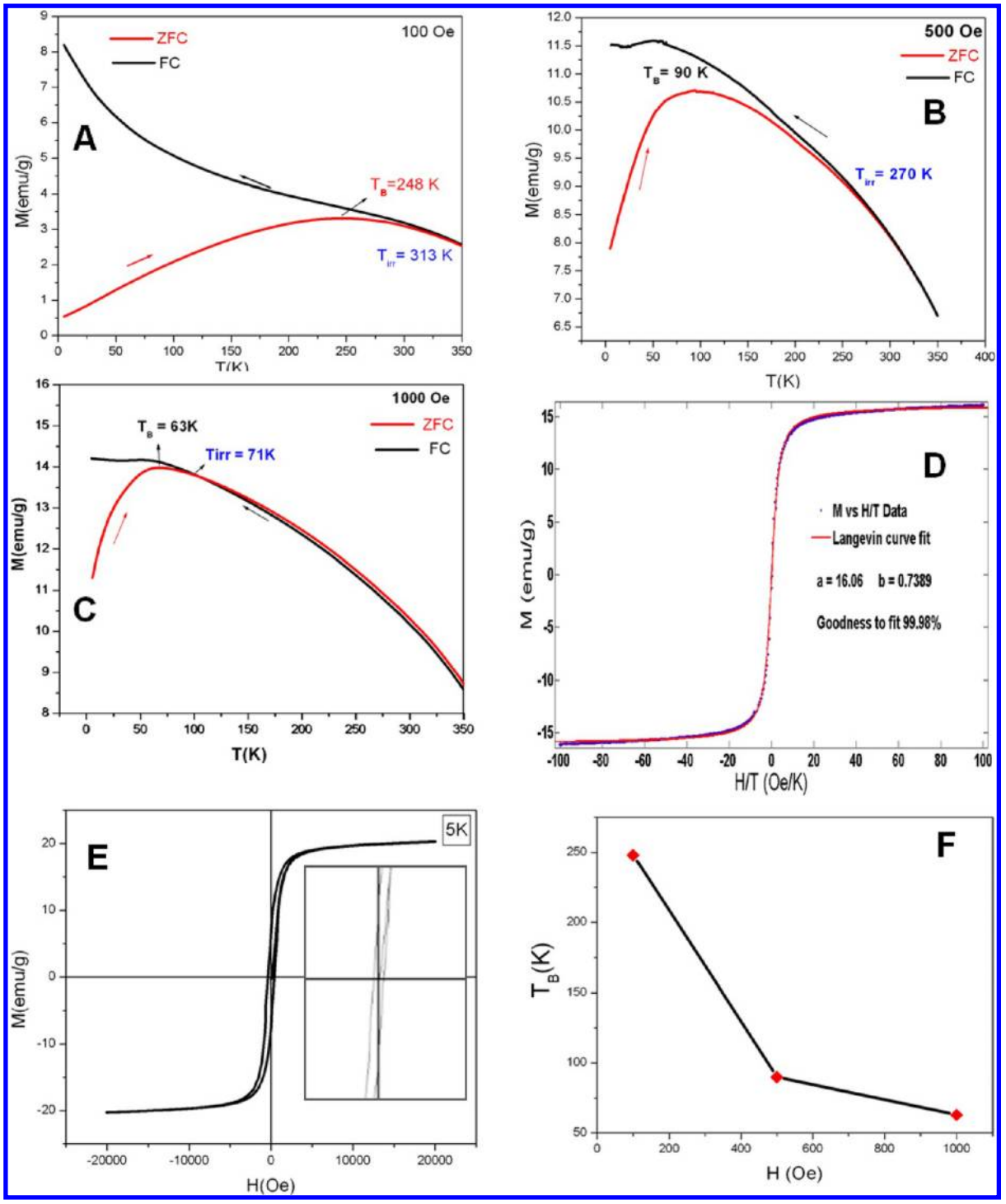

Figure 6. (A–F) Magnetic measurement of the FeAs nanoparticles. The ZFC–FC plot of magnetic susceptibility against temperature under an applied field of (A) 100 Oe; (B) 500 Oe and (C) 1000 Oe. (D) The Langevin fit for M/M_S vs H/T plots. (E) M vs H plot at 5 K showing a small coercivity. (F) Shows the dependence of T_B on the applied field.

in a narrow temperature range (350–600 K), and deviation outside that range is believed to be due to some complex exchange interactions and the presence of cooperative magnetism in the system.[14] To elucidate the magnetic behavior of these FeAs nanoparticles, magnetization as a function of temperature and applied field was investigated. The magnetization behavior as a function of temperature was measured under zero-field cooled (ZFC) and field-cooled (FC) condition with an applied field of 100–1000 Oe, and is plotted in Figure 6A–C. The absolute amount of Fe in these samples was obtained from AAS measurements (42.78 ppm), and all the magnetization data was normalized with respect to the estimated amount of FeAs in the sample (8.31 mg) rather than the total sample mass used for magnetic studies. A typical divergence of the ZFC–FC curve was observed in the M vs T plots, which is characteristic of several magnetic phenomena like superparamagnetism[33] and spin-glass behavior. Previous researchers have observed such divergence in the ZFC–FC

dx.doi.org/10.1021/cm303632c | *Chem. Mater.* 2013, 25, 1510–1518

plots for the pnictide nanoparticles and ascribed them to the superparamagnetic nature of the nanoparticles.[34−37] In such cases, the maximum in the ZFC plot is considered to be the blocking temperature (T_B), which was representative of the minimum temperature above which spontaneous fluctuations of the particle moment were allowed leading to loss of magnetic ordering. Superparamagnetism is characteristic in ferro- or ferrimagnetic systems when the material size is reduced below a critical dimension, such that it shows single magnetic domain. The presence of superparamagnetism in the nanoparticle ensemble is supported by two pieces of evidence. The first and foremost piece of evidence is that the magnetization as a function of H/T (H = applied field, T = temperature) for non-interacting single domain particles can be fitted to the Langevin equation (eq 1) as shown below.[38]

$$M = M_0\left[\coth\left(\frac{\mu H}{k_B T}\right) - \frac{1}{\left(\frac{\mu H}{k_B T}\right)}\right] \quad (1)$$

where M = magnetization, M_0 = saturation magnetization, H = applied magnetic field, μ = magnetic moment, T = temperature and k_B = Boltzmann constant. For the FeAs nanoparticles, the plot of M/M_0 vs H/T at different temperatures converges into one universal curve and could be fitted to the Langevin equation with a 99.98% accuracy as shown in Figure 6D. The second condition for superparamagnetic behavior is anhysteretic nature of the isothermal magnetization against applied field with zero coercivity and remanence, which also must be temperature independent above T_B.[39,40]

For the FeAs nanoparticles magnetization as a function of applied magnetic field was measured in the range 5−300 K as shown in Figure 6D and the Supporting Information (Figure S4) respectively. The absence of coercivity and remanence (i.e., the anhysteretic nature) in these plots was prominent above 77 K. Hence, from these magnetic characterizations it was concluded that these FeAs nanoparticles are indeed superparamagnetic with a fairly high T_B. There was no correspondence between the T_B and irreversibility temperature T_{irr} (T_{irr} = the temperature at which the ZFC and FC curves show divergence) (Figure 6A−C), indicating considerable size dispersion among the nanoparticles.[41] Typically the difference between the T_B and T_{irr} stems from the fact that all the nanoparticles in this system do not have identical energy barriers of magnetic reversal owing to their different sizes. This leads to a widening of the superparamagnetic transition over a temperature range where the divergence of the ZFC−FC curves (T_{irr}) and maxima of the ZFC curve (T_B) do not necessarily merge. As discussed previously from STEM and TEM studies these FeAs nanoparticles indeed show some size dispersity (10−15 nm). At lower temperatures, viz. 5 and 10 K, the magnetization plots show a very small coercivity (390 Oe), (Figure 6E), which might indicate very weak ferromagnetism in these particles or other short-range magnetic ordering like spin-glass.

In accordance with other superparamagnetic systems,[23] the T_B was dependent on the field applied, and T_B decreased with increasing magnetic field as shown in Figure 6F. A fairly high saturation magnetization of ∼18 emu/g was observed with these nanoparticles at low temperatures. However it should be noted that, at higher temperatures, the magnetization curve was still rising even above 20,000 Oe, indicating that the saturation magnetization will predictably be higher than that observed in the plots. In superparamagnetic nanoparticles, the T_B depends upon the size of the particles, the field applied and the experimental measuring time,[41] and is also influenced heavily by the extent of interparticle interactions. For the FeAs nanoparticles T_B as high as 240 K was observed at the lowest field of 100 Oe. There are many reasons and outcomes of such a high T_B in our system. Magnetocrystalline anisotropy and the higher critical radius of the nanoparticles contribute to the high T_B. It also implies that superparamagnetism can be avoided up to 240 K, which is a temperature closer to room temperature. Superparamagnets owing to their high magnetic moment are typically used in ferrofluids that may be used as magnetic inks, toners and frictionless seals.[42] Magnetic refrigeration is another application that uses superparamagnetic materials by reduction of surrounding temperature by heat absorption through magnetocaloric effect.[43] For most of these applications, a T_B close to room temperature is desired for increasing the efficiency of the device. Typically higher T_Bs are observed in alloy nanoparticles like Co@Au core shell nanoparticles (T_B = 290 K), Co@Cu (T_B = 235 K)[44] and Fe@Au core shell nanoparticles (170 K),[45] and mostly elaborate measures are required to inhibit interparticle interaction and increase the T_B to these values. Some of the measures include wrapping the nanoparticles with a spacer or nonmagnetic shell or dispersing them in a polymer matrix thereby diluting the interparticle interactions. Furthermore, it has been argued by Skumryev[46] that passivating such magnetic nanoparticles in an antiferromagnetic shell increases the T_B 30-fold, thereby beating the "superparamagnetic limit". In the present case, the as-synthesized FeAs nanoparticles being covered with a carbonaceous shell, by itself, presents a perfect assembly for decreasing the interparticle interactions thereby leading to inherently higher T_B. The carbonaceous shell around the magnetic FeAs nanoparticles also aids in pinning the magnetic moments within the nanoparticles. It also increases the chemical stability of FeAs@C nanoparticles toward surface oxidation.

Size Estimation of the FeAs Nanoparticles from Magnetic Characterization. For superparamagnetic nanoparticle ensembles above T_B, the Langevin fit can be also used for estimating the average particle volume by considering the following equations along with the Langevin equation (eq 1).

Expressing experimental magnetization as a function of H/T reduces eq 1 to the following form:

$$y = a\left[\coth(bx) - \frac{1}{(bx)}\right] \quad (2)$$

where $x = H/T$; $y = M$; $a = M_0$ and $b = \mu/k_B$.

$$\text{particle moment,} \quad \mu = M_S\langle V\rangle \quad (3)$$

where M_S = saturation moment of bulk FeAs; and $\langle V\rangle$ = average particle volume.

The theoretical saturation moment of bulk FeAs was calculated to be 93.9596 emu·g^{-1} by considering 2.2 unpaired electrons per Fe(III) atom in FeAs.[12] From the Langevin fit of the M vs H/T plot (Figure 6D), the parameters a and b could be obtained and eq 3 could be solved for $\langle V\rangle$ through proper substitution (the density of FeAs was taken as 7.721 g·cm^{-3} corresponding to the crystalline phase observed in the pxrd pattern). The average particle diameter obtained through this approach was approximately 8 nm, which was close to the

dx.doi.org/10.1021/cm303632c | Chem. Mater. 2013, 25, 1510−1518

average core size seen in these superparamagnetic particles through extensive SEM and STEM studies.

Previously Brock at al. have investigated a series of iron phosphide nanoparticles and have reported that the presence of trace amounts of Fe impurities in some of these nanoparticles interferes with the magnetic signal.[16] In our case however, we would like to underline the fact that at higher temperatures (above T_B) all the M vs H curves were anhysteretic in nature thereby ruling out the presence of any kind of bulk ferromagnetic impurities. Also, the nanoparticles obtained were mostly crystalline throughout as seen from the typical HRTEM image shown in Figure 3 thereby reducing the possibility of the presence of any unreacted Fe at the core. Careful elemental analysis through EDS and XPS failed to pick up any excess Fe and O signal from the edge of the nanoparticles, thereby minimizing the possibility of the presence of other Fe-containing impurities like Fe oxide at the surface of the nanoparticles. From the normalized magnetization data, we estimated that the amount of Fe impurity needed to generate a saturation moment as high as that observed in the nanoparticle sample (~18 emu/g at 5 K) was approximately 8% by weight (~0.736 mg Fe in 8.31 mg of sample). This limit is well above the detection limit of Mössbauer spectroscopy, which is considered to be the most sensitive technique for detection of Fe. Hence, Mössbauer spectroscopy was also performed on an ensemble of the FeAs@C nanoparticles to gain a better insight into the various oxidation states of Fe present in these nanoparticle samples and also to determine the presence/absence of metallic Fe as impurity.

Mossbauer Studies. The Mössbauer spectra collected from an ensemble of FeAs@C nanoparticles at room temperature and at 90 K showed a doublet with isomer shift of 0.5385 mm/s and a quadruple splitting of 0.4572 mm/s, which corresponds well with that of bulk FeAs containing Fe in the +3 oxidation state (Figures 7 and S5 in Supporting Information, respectively).[47] Fe in the zero oxidation state typically shows a sextet, which was not observed with the FeAs@C nanoparticles, thereby ruling out the presence of unreacted Fe at the core of these nanoparticles and extraneous Fe impurity. The close similarity between the spectra obtained from the nanoparticles and the bulk FeAs ruled out the presence of any other oxidation states of Fe as impurity in the nanoparticle sample. The peaks showed some broadening mainly due to the reduced size and polydispersity of these nanoparticles. We are presently trying to collect the Mössbauer spectra from these nanoparticles at temperatures below the T_B, such that we can gain a better insight into the magnetically ordered state of these nanoparticles.

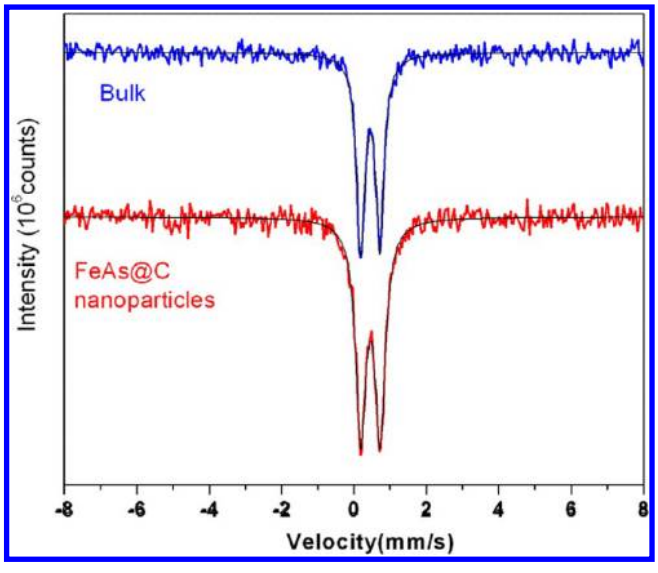

Figure 7. Mossbauer spectra of FeAs@C nanoparticles collected at room temperature showing a doublet characteristic of Fe(+3).

Mechanism. To gain an insight into the formation mechanism of FeAs@C nanoparticles, aliquots were collected at various times during the reaction and detailed microscopy was carried out to analyze the particle size and composition. It was observed that a spherical nanoparticle-like morphology was formed within the first hour of the reaction. The aliquot collected ~30 min after adding the $Fe(CO)_5$ ($t = 0$) contained similar core–shell morphology as seen at $t = 3$ h. However, the size of these nanoparticles was slightly smaller and more importantly As was more concentrated near the edges of the nanoparticle, while the core was Fe-rich (see Figure S3 in Supporting Information). From the EDS analysis it was evident that As concentration in the nanoparticles increased with the reaction time and the concentration of As moved from near the periphery of the nanoparticles toward the core with progress of the reaction. The size of the nanoparticles between different aliquots collected at different stages of growth did not show a large variation indicating that spontaneous nucleation and diffusion controlled growth were predominant factors under the reaction conditions.

On the basis of simple organometallic and coordination chemistry it can be expected that, during initial stage of the chemical reaction, ligand exchange takes place as soon as $Fe(CO)_5$ is added into the mixture of TPA and HDA. The CO ligand is displaced by the $As(C_6H_5)_3$ to form an intermediate complex $[(C_6H_5)_3As{-}Fe(CO)_4]$ and free CO, generated according to eq 4. This kind ofligand exchange with phosphines

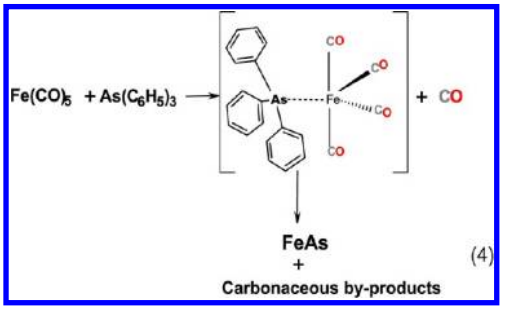

and arsines is very favorable since they act as electron donating Lewis bases.[48] In principle, the intermediate can behave as a single source precursor for both Fe and As thus facilitating the reaction between these two precursors without the need for a catalyst. A single source precursor which has all the elements of the product composition in one single molecule is very advantageous and has been widely used in nanomaterials synthesis.[49] In this case, the intermediate brings the As and Fe closer than would be expected from the traditional solid state methods of FeAs synthesis. Proximity of As and Fe in this intermediate renders the possibility of an internal redox between As and Fe. The driving force is difference in the reduction potentials of Fe^{3+}/Fe and As^{3+}/As^{3-} couples as shown in eqs 5 and 6 respectively. The presence of amine (HDA) in the mixture makes the medium slightly basic, thereby

dx.doi.org/10.1021/cm303632c | Chem. Mater. 2013, 25, 1510–1518

decreasing the reducing ability of the arsine compound. Since As^{3+}/As^{3-} has a more positive reduction potential, it acts as a stronger oxidizing agent thereby oxidizing Fe(0) to Fe^{3+} while itself being reduced to As^{3-}. The overall change in potential for this redox reaction is +1.113 V as calculated by using eqs 5 and 6.[50] The positive value of ΔE indicates that this reaction will be spontaneous since the change in internal free energy would be negative.

$$Fe^{3+} \rightarrow Fe(0) + 6e, \quad E^{\circ}_{[Fe(3+)/Fe(0)]} = -0.768\ V \tag{5}$$

$$As^{3+} + 6e^{-} \rightarrow As^{3-}, \quad E^{\circ}_{[As(3+)/As(3-)]} = +0.345\ V \tag{6}$$

Further importance of the basic medium was demonstrated by the use of oleic acid (5 mM) as surfactant instead of HDA which failed to produce FeAs nanoparticles from $Fe(CO)_5$ and TPA. Temperature also plays a definitive role in this ligand exchange and internal redox, since it is observed that, at low temperature, the product contains a mixture of FeAs and $FeAs_2$ (which contains Fe in the +2 oxidation state).

The following hypothesis is being made to explain the morphological conversion of the nanoparticles. At $t = 0$, there is a burst of nucleation due to addition of $Fe(CO)_5$ forming Fe-rich nuclei capped with HDA. TPA starts reacting at the surface of the nuclei, and the initial layers of FeAs formed (presumably through decomposition of the single source precursor as shown in eq 4) coat the nuclei. At conditions of constant high temperature (300 °C) As diffuses deeper into the nuclei thereby promoting further conversion of the core to FeAs. The growth front of FeAs starts at the periphery of the nuclei and moves inward, somewhat similar to the inside-out growth mechanism seen in inorganic fullerenes.[51] As time approaches t = 3 h, the entire core has been converted into FeAs. A pictorial representation of this growth mechanism is shown in Figure 8.

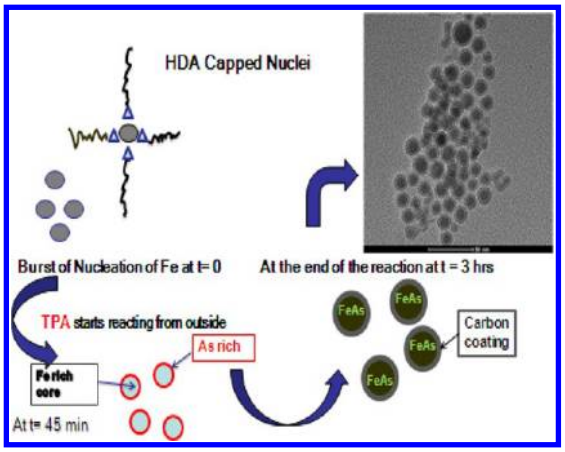

Figure 8. Proposed growth mechanism of the FeAs@C nanoparticles.

The carbonaceous shell formation starts from the very preliminary stages of growth. The presence of carbon rich species in the form of ligands and reactants (e.g., CO in $Fe(CO)_5$, 3 phenyl rings in TPA and the C_{16} chain in HDA) contributed to the formation of the carbonaceous shell through decomposition of the molecular precursors. Previous researchers working with TPA have also proposed that the pyrogenation of TPA generates biphenyls,[26] and the decomposition of these aromatic rings under the refluxing conditions can lead to the formation of the carbonaceous shell. The enhanced catalytic activity of Fe toward pyrolysis of the hydrocarbons has been well studied through the formation of carbon nanotubes and nanofibers.[52] In the present case it can be expected that the presence of Fe-containing precursor facilitated the formation of the carbonaceous shell as has been recently observed by the authors.[53]

CONCLUSION

We have successfully synthesized pure FeAs@C core−shell nanoparticles by a simple, single step solution based method. These nanoparticles showed superparamagnetism with a T_B as high as 240 K and hence may find possible applications as ferrofluids and magnetic recording materials and serve as model systems for understanding helimagnetism at the nanoscale. The conversion of a helimagnet to a superparamagnet by reducing size provides us with a perfect practical example of a system where nanostructuring brings a change in the bulk properties. The magnetic exchange interactions in FeAs are complex, and these kinds of findings might provide crucial tools for better understanding of the spin interactions in the pnictide layers in nanostructured geometry as well as the pnictide superconductors since their properties depend on the magnetic interactions of the pnictide layer. These FeAs nanoparticles also bring us one step closer in synthesizing the novel iron arsenide based superconducting nanostructures like the LiFeAs. We are currently trying to incorporate Li into the FeAs nanoparticles through sacrificial template approach. The synthesis method reported here is a very simple, soft chemical approach which is facilitated by the ligand exchange capabilities of the arsine based ligands, and can be generalized for synthesizing nanostructures of other arsenides. In our preliminary research we have been able to make nanostructures of other arsenides like CoAs, CrAs, MnAs and InAs by employing the above methodology. The solution based approach also provides opportunities for introducing dopants in the nanostructure and also induces anisotropic growth by using suitable catalysts through SLS growth techniques.

ASSOCIATED CONTENT

Supporting Information

PXRD pattern, M vs H (hysteresis curves), nanoparticle histogram, EDS line scan and low temperature Mössbauer spectra. This material is available free of charge via the Internet at http://pubs.acs.org.

AUTHOR INFORMATION

Corresponding Author

*E-mail: nathm@mst.edu.

Present Address

[‖]K.S. is presently at FEI Company, 5350 NE Dawson Creek Drive, Hillsboro, Oregon 97124.

Author Contributions

[‡]P.D. and M.N. contributed equally.

Notes

The authors declare no competing financial interest.

ACKNOWLEDGMENTS

The authors would like to acknowledge MRC for the equipment access, Jay Switzer (Chemistry, Missouri S&T) for magnetic measurements, Amitava Choudhury (Chemistry, Missouri S&T) for Mössbauer spectroscopy, Kartik Ghosh (Missouri State University, Springfield) for magnetic character-

izations, Richard Brow (MRC) for Raman spectroscopy and Thomas Vojta, Physics, Missouri S&T, for helpful discussions.

REFERENCES

(1) Kamihara, Y.; Hiramatsu, H.; Hirano, M.; Kawamura, R.; Yanagi, H.; Kamiya, T.; Hosono, H. *J. Am. Chem. Soc.* **2006**, *128*, 10012.
(2) Matsuishi, S.; Hosono, H. *Mater. Integr.* **2011**, *24*, 42.
(3) Kamihara, Y.; Watanabe, T.; Hirano, M.; Hosono, H. *J. Am. Chem. Soc.* **2008**, *130*, 3296.
(4) Johrendt, D.; Pottgen, R. *Angew. Chem., Int. Ed.* **2008**, *47*, 4782 and references therein.
(5) Chen, X. H.; Wu, T.; Wu, G.; Liu, R. H.; Chen, H.; Fang, D. F. *Nature* **2008**, *453*, 761.
(6) Torikachvili, M. S.; Bud'ko, S. L.; Ni, N.; Canfield, P. C. *Phys. Rev. Lett.* **2008**, *101*, 057006(4).
(7) Rotter, M.; Tegel, M.; Johrendt, D.; Schellenberg, I.; Hermes, W.; Pöttgen, R. *Phys. Rev. B* **2008**, *78*, 020503/1.
(8) Zhang, S. J.; Wang, X. C.; Sammynaiken, R.; Tse, J. S.; Yang, L. X.; Li, Z.; Liu, Q. Q.; Desgreniers, S.; Yao, Y.; Liu, H. Z.; Jin, C. Q. *Phys. Rev. B* **2009**, *80*, 014506(1).
(9) Alireza, P. L.; Ko, Y. T. C.; Gillett, J.; Petrone, C. M.; Cole, J. M.; Lonzarich, G. G.; Sebastian, S. E. *J. Phys.: Condens. Matter* **2009**, *21*, 012208.
(10) Hosono, H. *J. Phys. Soc. Jpn.* **2008**, *77* (Suppl. C), 1.
(11) Hase, I.; Yanagisawa, T. *Phys. C (Amsterdam, Neth.)* **2010**, *470*, 538.
(12) Shirai, M. *Phys. E (Amsterdam, Neth.)* **2001**, *10*, 143. Segawa, K.; Ando, Y. *J. Phys. Soc. Jpn.* **2009**, *78*, 104720.
(13) Selte, K.; Kjekshus, A. *Acta Chem. Scand.* **1969**, *23*, 204.
(14) Selte, K.; Kjekshus, A.; Andresen, A. F. *Acta Chem. Scand.* **1972**, *26*, 3101.
(15) Jeffries, J. R.; Butch, N. P.; Cynn, H.; Saha, S. R.; Kirshenbaum, K.; Weir, S. T.; Vohra, Y. K.; Paglione, J. *Phys. Rev. B: Condens. Matter Mater. Phys.* **2011**, *83*, 134520/1.
(16) Muthuswamy, E.; Kharel, P. R.; Lawes, G.; Brock, S. L. *ACS Nano* **2009**, *3*, 238.
(17) Park, J.; Koo, B.; Yoon, K. Y.; Hwang, Y.; Kang, M.; Park, J. G.; Hyeon, T. *J. Am. Chem. Soc.* **2005**, *127*, 8433.
(18) Yang, Li; Malik, A. M.; O'Brien, P. *J. Am. Chem. Soc.* **2005**, *127*, 16020.
(19) Qian, C.; Franklin, K.; Ma, L.; Tsui, F.; Yang, P.; Liu, J. *J. Am. Chem. Soc.* **2004**, *126*, 1195.
(20) Muthuswamy, E.; Savithra, G. H. L.; Brock, S. L. *ACS Nano* **2011**, *5*, 2402.
(21) Perera, S. C.; Tsoi, G.; Wegner, L. E.; Brock, S. L. *J. Am. Chem. Soc.* **2003**, *125*, 13960.
(22) Tian, P.; Zhang, Y.; Senevirathne, K.; Brock, S. L.; Dixit, A.; Lawes, G.; Billinge, S. J. L. *ACS Nano* **2011**, *5*, 2970.
(23) Lu, J.; Xie, Y.; Jiang, X.; He, W.; Du, G. *J. Mater. Chem.* **2001**, *11*, 3281.
(24) Zhang, X. M.; Wang, C.; Qian, X. F.; Xie, Y.; Qian, Y. T. *J. Solid State Chem.* **1999**, *144*, 237.
(25) Afzaal, M.; Malik, A. M.; O'Brien, P. *Chem. Rev.* **2010**, *110*, 4417.
(26) Wang, J.; Yang, Q. *Dalton Trans.* **2008**, 6060.
(27) Wang, J.; Yang, Q. *Chem. Lett.* **2008**, *37*, 306.
(28) Recoil software: Lagarec, K.; Rancourt, D. G. *Nucl. Instrum. Methods Phys. Res., Sect. B* **1997**, *129*, 266.
(29) Patterson, A. L. *Phys. Rev.* **1939**, *56*, 978.
(30) Schaufelberger, F. A. *J. Met.* **1956**, *8*, 695.
(31) Choi, H. C.; Jung, Y. M.; Kim, S. B. *Vib. Spectrosc.* **2005**, *37*, 33.
(32) Ferarri, A. C.; Robertson, J. *Phys Rev. B* **2000**, *61*, 14095.
(33) Rondinone, A. J.; Samia, A. C. S.; Zhang, Z. J. *J. Phys. Chem. B* **1999**, *103*, 6876.
(34) Mikhaylova, M.; Kim, D. K.; Bobrysheva, N.; Osmolowsky, M.; Semenov, V.; Tsakalakos, T.; Muhammed, M. *Langmuir* **2004**, *20*, 2472.
(35) Yun-Hao, X.; Jian-Ping, W. *IEEE Trans. Magn.* **2007**, *43*, 3109.
(36) Bala, T.; Bhame, S. D.; Joy, P. A.; Prasad, B. L. V.; Sastry, M. *J. Mater. Chem.* **2004**, *14*, 2941−2945.
(37) Zelenakova, A.; Zelenak, V.; Degmova, J.; Kovac, J.; Sedlackova, K.; Kusy, M.; Sitek, J. *Rev. Adv. Mater. Sci.* **2008**, *18*, 501−504.
(38) Knobel, M. N.; W.C.; Socolovsky, L. M.; De Biasi, E.; Vargas, J. M.; Denardin, J. C. *J. Nanosci. Nanotechnol.* **2008**, *8*, 2836−2857.
(39) Unruh, K.; Chien, C. *Nanomaterials; Synthesis, Properties and Applications*; Edelstien, A., Cammarata, C., Eds.; Taylor and Francis: New York, 1996; pp 352−359.
(40) Lu, A. H.; Salabas, E. L.; Schuth, F. *Angew. Chem., Int. Ed.* **2007**, *46*, 1222−1244.
(41) Opel, M.; Nielsen, K. W.; Bauer, S.; Goennenwein, S. T. B.; Cezar, J. C.; Schmeisser, D.; Simon, J.; Mader, W.; Gross, R. *Eur. Phys. J. B* **2008**, *63*, 437.
(42) Lee, W. R.; Kim, M. G.; Choi, J.-R.; Park, J.-I.; Ko, S. J.; Oh, S. J.; Cheon, J. *J. Am. Chem. Soc.* **2005**, *127*, 16090.
(43) Raj, K.; Moskowqitz, R. *J. Magn. Magn. Mater.* **1990**, *85*, 233.
(44) McMichael, R. D.; Shull, R. D.; Swartzendruber, L. J.; Bennett, L. H.; Watson, R. E. *J. Magn. Magn. Mater.* **1992**, *111*, 29.
(45) Zhang, J.; Post, M.; Veres, T.; Jakubek, Z. J.; Guan, J.; Wang, D.; Normandin, F.; Deslandes, Y.; Simard, B. *J. Phys. Chem. B* **2006**, *110*, 7122.
(46) Skumryev, V.; Stoyanov, S.; Zhang, Y.; Hadjipanayis, G.; Givord, D.; Nogues, J. *Nature* **2003**, *423*, 850.
(47) Kulshreshtha, S. K.; Raj, P.; Rao, U. R. K. *Proc. Nucl. Phys. Solid State Phys. Symp.* **1973**, *16*, 316.
(48) Crabtree, R. H. *The Organometallic Chemistry of the Transition Metals*; Wiley: 2001; p 96.
(49) Smith, K. D; Luther, M. J; Semonin, E. O; Nozik, J. A; Matthew C. Beard, C. B. *ACS Nano* **2011**, *5*, 183.
(50) Bard, A. J.; Parsons, R.; Jordan, J. *Standard Potentials in Aqueous Solutions*; IUPAC (Marcel Dekker): New York, 1985.
(51) Feldman, Y. W., E.; Srolovitz, D. J.; Tenne, R. *Science* **1995**, *267*, 222.
(52) Dündar-Tekkaya, E.; Karatepe, N. *World Acad. Sci., Eng. Technol.* **2011**, No. 55, 225−231.
(53) Mishra, S.; Song, K.; Koza, J. A.; Nath, M. *ACS Nano* **2013**, *7*, 1045.